IJMMM International Journal of Minerals, Metallurgy and Materials 矿物冶金与材料学报（英文版）

Effect of the surface microstructure of arsenopyrite on the attachment of *Sulfobacillus thermosulfidooxidans* in the presence of dissolved As()

Zhen Xue, Zhen-yuan Nie, Hong-chang Liu, Wei-bo Ling, Qian Pan, Jin-lan Xia, Lei Zheng, Chen-yan Ma, and Yi-dong Zhao

Cite this article as:
Zhen Xue, Zhen-yuan Nie, Hong-chang Liu, Wei-bo Ling, Qian Pan, Jin-lan Xia, Lei Zheng, Chen-yan Ma, and Yi-dong Zhao, Effect of the surface microstructure of arsenopyrite on the attachment of *Sulfobacillus thermosulfidooxidans* in the presence of dissolved As(), *Int. J. Miner. Metall. Mater.*, 28(2021), No. 7, pp. 1135-1144. https://doi.org/10.1007/s12613-020-2231-9

View the article online at SpringerLink or IJMMM Webpage.

International Journal of Minerals, Metallurgy and Materials
Volume 28, Number 7, July 2021, Page 1135
https://doi.org/10.1007/s12613-020-2231-9

Effect of the surface microstructure of arsenopyrite on the attachment of *Sulfobacillus thermosulfidooxidans* in the presence of dissolved As(Ⅲ)

Zhen Xue[1)], *Zhen-yuan Nie*[1,2)], *Hong-chang Liu*[1,2)], *Wei-bo Ling*[1)], *Qian Pan*[1)], *Jin-lan Xia*[1,2)], *Lei Zheng*[3)], *Chen-yan Ma*[3)], *and Yi-dong Zhao*[3)]

1) School of Minerals Processing and Bioengineering, Central South University, Changsha 410083, China
2) Key Lab of Biometallurgy of Ministry of Education of China, Central South University, Changsha 410083, China
3) Beijing Synchrotron Radiation Facility, Institute of High Energy Physics, Chinese Academy of Sciences, Beijing 100049, China
(Received: 25 August 2020; revised: 3 November 2020; accepted: 27 November 2020)

Abstract: Understanding bacterial adsorption and the evolution of biofilms on arsenopyrite with different surface structures is of great significance to clarifying the mechanism of microbe–mineral interfacial interactions and the production of acidic mine drainage impacting the environment. In this study, the attachment of *Sulfobacillus thermosulfidooxidans* cells and subsequent biofilm formation on arsenopyrite with different surface structures in the presence of dissolved As(Ⅲ) was studied. Arsenopyrite slices with a specific surface were obtained by electrochemical corrosion at 0.26 V. The scanning electronic microscopy-energy dispersion spectra analyses indicated that the arsenopyrite surface deficient in sulfur and iron obtained by electrochemical treatment was not favorable for the initial adsorption of bacteria, and the addition of As(Ⅲ) inhibited the adsorption of microbial cells. Epifluorescence microscopy showed that the number of cells attaching to the arsenopyrite surface increased with time; however, biofilm formation was delayed significantly when As(Ⅲ) was added.

Keywords: arsenopyrite; surface microstructure; bioleaching; *sulfobacillus thermosulfidooxidans*; attachment behaviors

1. Introduction

Arsenopyrite (FeAsS) is the most abundant material containing arsenic and is often found in a range of ore deposits such as high temperature hydrothermal deposits, pegmatite, and metasomatic deposits [1]. Gold and silver are usually encased in FeAsS [2–3]. As a result, FeAsS is often mined in the Au and Ag extraction industries. The decomposition of arsenic-bearing gold ore by bacterial oxidation to expose gold grains is known as biological pre-oxidation. Recent research has focused on bacterial oxidation because of its environmental friendliness, ease of operation, and low cost [4]. Under oxidizing conditions and interactions with microorganisms, arsenic and sulfur from arsenopyrite are released into the environment, resulting in a high concentration of dissolved As in acid mine drainage (AMD) [5] that can negatively impacting the environment.

Multiphase interfacial interactions, such as microbe–mineral, mineral–mineral, and microbe–solution–mineral, are involved in the bioleaching of minerals [6]. During biodissolution of minerals, macro phenomena, such as precipitation and transformation, occur which often results from micro-scale interactions between microbes and minerals. The interfacial interaction between a microbe and mineral is the main process of bioleaching, and it is closely related to the physical and chemical properties of the mineral surface, the structural composition of the mineral, the topography of the exposed outer surface, and the type of microorganism. The interfacial interaction between a microbe and mineral is affected by the microstructure of the mineral surface [7]. The physical properties of the mineral surface are strongly influenced by the microstructure and interfacial interaction between the microbe and mineral [8–12].

Microbial attachment is the key to mineral–microbe interaction, and studies have shown that adsorbed microorganisms are more effective than free microorganisms in promoting mineral dissolution [13]. Previous studies also indicated that the chemical speciation and microstructure of the mineral surface play an important role in the selective attachment of microorganisms. For example, Lara *et al*. [14–15] studied the relationship between the attachment of *Acidithiobacillus thiooxidans* on chalcopyrite and pyrite surfaces treated elec-

Corresponding authors: Hong-chang Liu E-mail: hongch_liu@csu.edu.cn; Jin-lan Xia E-mail: jlxia@csu.edu.cn

trochemically and surface sulfur speciation, illustrating that the cells were more spread on the surface containing S^0 than on the surface containing S_n^{2-} or CuS. However, the microscale interfacial interaction between the microbe and arsenopyrite, particularly the adsorption behavior on the surface of arsenopyrite, is rarely studied [16].

Alternatively, the adsorption of microorganisms on the mineral surface is affected by the chemical speciation, element distribution, physical structure of the mineral surface, and various environmental factors such as temperature, pH, and toxic element concentration [17]. For example, the presence of toxic As and Hg can affect the formation of biofilm by the structure of the organic matter of the biofilm [18–20]. Ramírez-Aldaba *et al*. [16] recently demonstrated that supplementary As(V) could change the hydrophilicity and decrease the production of the extracellular surface proteins of the biofilm on the arsenopyrite surface. Arsenic is a toxic quasi-metallic element often associated with minerals. Arsenic has three valence states (−3, +3, and +5) and multiple forms, in which the inorganic As in trivalent form has much greater toxicity than the other forms [21]. A detailed evaluation considering the effect of an adverse environment on the bacterial attachment properties during arsenopyrite bioleaching in the presence of dissolved As(Ⅲ), and its influence on the formation and evolution of biofilm need to be studied to understand the effect of As(Ⅲ) on the interaction between arsenopyrite and a microorganism.

In this study, the attachment behavior and biofilm formation of moderately thermophilic *Sulfobacillus thermosulfidooxidans* on the surface of electrochemically treated arsenopyrite were investigated. The effect of an additional amount of dissolved As(Ⅲ) on the bacteria attachment of arsenopyrite, the evolution of biofilm, and a change in the chemical speciation on the mineral surface were also evaluated. These studies are meaningful to understanding the microbe–mineral interfacial interaction and the leaching process reactions of arsenopyrite in the presence of As(Ⅲ) in industrial and natural environments.

2. Experimental

2.1. Materials

2.1.1. Mineral samples

The arsenopyrite sample was obtained from Guangxi Province, China. The X-ray diffraction (XRD) of the pristine arsenopyrite was analyzed using an X-ray diffractometer (DX 2000, Dandong Fangyuan Instrument Co. Ltd., China) with Cu K_α radiation (λ = 0.154 nm), and the result shows that arsenopyrite is the main phase (Fig. 1). X-ray fluorescence spectroscopy shows that the main elements of the mineral sample were (wt%): As 45.09, Fe 34.80, S 14.57, O 2.25, Si 1.44, Al 0.53, Cu 0.32, Pb 0.26, and Sn 0.23. The content of As, Fe, and S were approximate to ideal results.

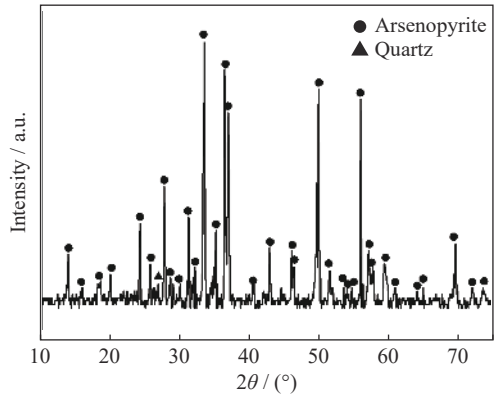

Fig. 1. The XRD pattern of the arsenopyrite sample.

2.1.2. Strain and culture medium

The moderately thermophilic *S. thermosulfidooxidans* YN22 (accession number of 16S rDNA in GenBank: DQ650351) was provided by the Key Lab of Biometallurgy of Ministry of Education, Central South University, China, and the 16S rDNA analysis shows the strain is pure [22]. The strain is a spore-forming facultative autotrophic bacterium that is capable of utilizing Fe^{2+}, S^0, and sulfides as energy sources [23–25]. Its optimum growth is at approximately 45°C with a pH of 1.9–2.4 [26–28]. Prior to the experiment, *S. thermosulfidooxidans* was cultured for several generations in 9K medium with 10 g/L FeAsS as the only energy source at 45°C and an initial pH 1.8 [23]. The cells were collected at the logarithmic growth stage by centrifugation at 10000*g* for 5 min, and then washed twice with electrolyte (9K medium) to obtain relatively pure bacteria. The 9K medium consisted of the following components (per liter): $(NH_4)_2SO_4$ 1.5 g, KH_2PO_4 0.25 g, $MgSO_4{\cdot}7H_2O$ 0.25 g, and $CaCl_2{\cdot}2H_2O$ 0.01 g, and yeast extract 0.2 g.

2.2. Methods

2.2.1. Electrochemical experiments

Electrochemical experiments were performed using a potentiostat PAR 283 (EG&G, Gaithersburg, MD, USA), including forward and reverse cyclic voltammetry (CV) and potentiostatic corrosion according to Ling *et al*. [7]. A 500 mL glass electrochemical cell with a three-electrode system was adopted, i.e., arsenopyrite working electrode, graphite rod counter electrode, and a saturated silver chloride (AgCl/Ag) reference electrode [29].

The arsenopyrite working electrode was prepared as follows: natural arsenopyrite samples were cut by a JKJQ-300 rock slicer (Taizhou Qiangtai Machinery Factory, China) to obtain a cylindrical section (12–15 mm in diameter and ~5 mm in thickness) without obvious defects. Each arsenopyrite slice was mounted in a polytetrafluorethylene matrix, and sequentially polishing with different grades of silicon carbide paper from 200 to 3500 mesh. The slices were rinsed three times with ethanol and distilled water before the electro-

chemical experiments [7].

The electrolyte was 9K medium free of O_2 (to be completed by filling with N_2 (99.999%)), and the pH was adjusted to 1.8 by H_2SO_4 [7]. All electrochemical experiments were conducted in 9K medium. The three electrodes and electrolyte were placed in a water thermostat system to maintain the temperature.

2.2.2. Bioleaching experiments

Bioleaching experiments were performed on a rotary shaker at 45°C and 170 r/min with 100 mL 9K medium in 250 mL Erlenmeyer flasks. The initial concentration of *S. thermosulfidooxidans* cells and initial pH was 1.0×10^8 cells/mL and 1.8 (adjusted by H_2SO_4). Three groups of bioleaching experiments were prepared according to the addition of arsenopyrite slices and/or As(III): (1) $FeAsS_{untreated}$ group with untreated arsenopyrite slices; (2) $FeAsS_{treated}$ group with electrochemically treated arsenopyrite slices; and (3) $FeAsS_{treated}$_As(III) group with electrochemically treated arsenopyrite slices and $NaAsO_2$. The arsenopyrite slice samples were removed at 1, 48, 120, and 200 h and stored under nitrogen at −80°C until further analyses. Each experiment was performed in triplicate at the same condition, and the results were presented as averages.

During bioleaching, the pH was determined by a pH meter (PHS-3C), and the redox potential (ORP) was determined using a platinum (Pt) electrode with an $Hg/HgCl_2$ reference electrode [24]. The pH and ORP results at 0 h were measured immediately after the addition of different arsenopyrites slices, *S. thermosulfidooxidans*, and As(III).

2.2.3. Attachment behavior analysis

The attachment behavior of *S. thermosulfidooxidans* on different arsenopyrite surfaces was studied at the initial attachment stage and biofilm formation stage by scanning electronic microscopy-energy dispersion spectra (SEM–EDS, Quanta FEG 250, FEI, Thermo Fisher Scientific, Hillsboro, OR, USA) and epifluorescence microscope (EFM, DM2500, Leica, Buffalo Grove, IL, USA), respectively [7]. The number of cells initially attached to the arsenopyrite surface was determined by the carbon atom amount (at%). The formation and evolution of biofilm was observed by staining with fluorescein isothiocyanate (FITC) and 4′6-diamidino-2-phenylindole (DAPI) [30–32]. For each EDS result, at least six spots were used for statistical analysis.

2.2.4. Surface structure and chemical speciation analyses

During bioleaching, the surface morphology and elemental composition of arsenopyrite were analyzed by SEM/EDS, and the S speciation transformation on the arsenopyrite surface was characterized by S K-edge XANES spectroscopy. The S K-edge XANES spectra were recorded at 4B7A beamline, Beijing Synchrotron Radiation Facility (BSRF), Beijing, China. The relevant samples were evaluated in fluorescence mode at ambient temperature and scanned at a step width of 0.2 eV from 2460 to 2510 eV [33]. The XANES spectra were normalized [34] and fitted by the IFEFFIT program with the linear combination of the standard reference spectra, and the fitting results were obtained [35].

3. Results

3.1. Characterization of the surface structure of arsenopyrite after electrochemical treatment

The surface morphology of the arsenopyrite treated electrochemically changed obviously at 0.26 V (Fig. 2), which determined by the results of previous studies. The normalized molecular formula of several regions on the arsenopyrite surface according to the elemental composition, indicating untreated regions of $Fe_{1.32}AsS_{0.80}$, and regions treated 0.26 V were $Fe_{1.02}AsS_{0.54}$ (Table 1), indicating obvious S and Fe defects on the arsenopyrite surface treated with 0.26 V. According to previous publications [7,11,29], the effect of the electrochemical corrosion on the mineral surface was significant for both microstructure and chemical speciation.

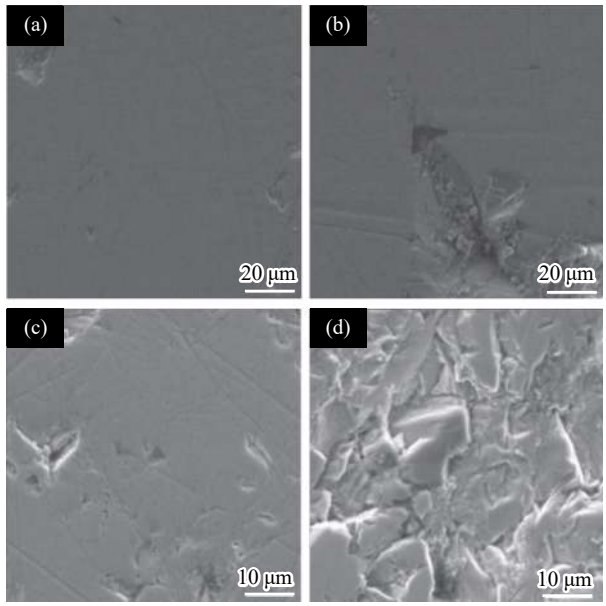

Fig. 2. SEM images of the surface of the FeAsS slice (a, c) and FeAsS slice (b, d) treated electrochemically at 0.26 V: (a, b) smooth area; (c, d) gully region.

3.2. Variation of pH and redox potential

The changes of pH and ORP values in different systems during bacterial attachment with time are shown in Fig. 3. The pH value of all the three groups increased initially (< 48 h), then decreased with time (> 48 h). The pH of the group with $NaAsO_2$ was much greater than that of the other two groups at 0 h, indicating the consumption of H^+ with the addition of $NaAsO_2$. The pH of the FeAsS group and $FeAsS_{treated}$ group were also different, i.e., the pH for the latter in-

Table 1. The normalized EDS results of As, Fe, and S and atom percent (at%) of elemental carbon (C) for different arsenopyrite surfaces with different bioleaching times

Time / h	FeAsS		$FeAsS_{treated}$		$FeAsS_{treated}$_As(III)	
	Normalized results	C / at%	Normalized results	C / at%	Normalized results	C / at%
0	$Fe_{1.32}AsS_{0.80}$	0	$Fe_{1.02}AsS_{0.54}$	0	$Fe_{1.02}AsS_{0.54}$	0
1	$Fe_{1.11}AsS_{0.55}$	7	$Fe_{0.95}AsS_{0.57}$	6.51	$Fe_{0.97}AsS_{0.63}$	4.85
48	$Fe_{1.90}AsS_{0.75}$	14.37	$Fe_{1.02}AsS_{0.71}$	12.06	$Fe_{0.98}AsS_{0.67}$	8.35
120	$Fe_{1.62}AsS_{0.76}$	18.63	$Fe_{1.05}AsS_{0.88}$	20.88	$Fe_{1.08}AsS_{0.62}$	13.70
200	$Fe_{1.14}AsS_{0.82}$	24.51	$Fe_{1.05}AsS_{0.84}$	20.95	$Fe_{0.97}AsS_{0.64}$	18.55

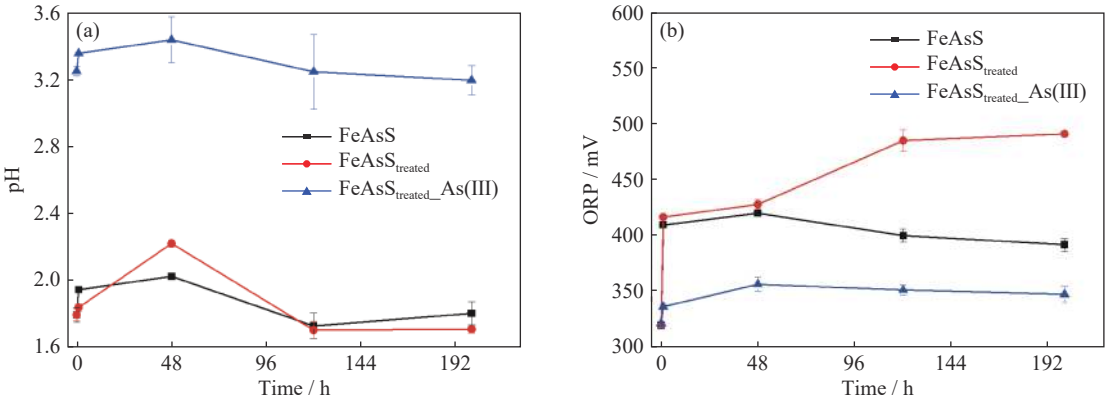

Fig. 3. Changes of pH (a) and ORP (b) during bacteria adsorption.

creased more at 48 h and decreased more at 120–200 h. The increase of pH indicates that the initial process was dominated by acid consumption. After 48 h, the generated acid was more than the consumed acid, causing a gradual decrease in the pH.

The ORP changes of the three groups were quite different. Both the FeAsS group and $FeAsS_{treated}$_As(III) showed a trend of increasing and then decreasing, while the ORP of the $FeAsS_{treated}$ group increased continuously. The ORP value of the $FeAsS_{treated}$ group was significantly greater than that of the $FeAsS_{treated}$_As(III) group, which may be because of the deficiency in S and Fe on the surface after the electrochemical treatment that is more conducive to bacterial attachment and promoting the interaction between bacterial cells and minerals to release more Fe^{3+}. Therefore, the ORP continued to increase.

3.3. SEM–EDS results

Fig. 4 and Table 1 showed the change in surface morphology and elemental composition in the physical adsorption (for 1 h) and the late adsorption of bacteria on arsenopyrite, respectively.

For the control group (Figs. 4(a)–4(d)), he attachment of bacteria mainly occurred on the arsenopyrite surface at 1 h. At 48 h, small pieces of biofilm appeared, and at 200 h, the biofilm covered the surface of the arsenopyrite slice. Figs. 4(e–h) and 4(i–l) show that the adsorption sites of bacteria are mainly concentrated in the gully/groove area. During the initial adsorption period (1 h), there was bacterial adsorption on the surface of arsenopyrite with electrochemical treatment (Fig. 4(e)); however, there were few bacteria. At 48 h, obvious adsorption could be observed, and the biofilm tend to be tighter. However, for the group of electrochemical treatment with As(III), there was no significant adsorption initially (1 h) and then the cell accumulation was not visible.

The change in the normalized elemental composition ($Fe_xAs_yS_z$) and the content of bacterial cells (in terms of carbon percentage, at%) on the arsenopyrite surface for two groups of electrochemical corrosion are shown in Table 1. The elements of these three groups were obviously different. The content of C increased from 1 to 200 h. Before 48 h, the cell quantities on the arsenopyrite slices were FeAsS > FeAsS treated > FeAsS treated and with As(III), which means that in the early stage, a surface deficient in S was unfavorable for the initial adsorption in the bioleaching.

3.4. Changes in cell attachment and biofilm formation on the arsenopyrite surfaces

The attachment of bacterial cells labeled by FITC and DAPI at different times during bioleaching are shown in Fig. 5 and Fig. 6, respectively.

The number of green spots (FITC-labeled bacteria) in the three arsenopyrite systems all increased with leaching time Figs. 5(a)–5(d) show the adsorption of *S. thermosulfidooxidans* on the surface of untreated arsenopyrite. The adsorption number of bacteria cells on the arsenopyrite surface in-

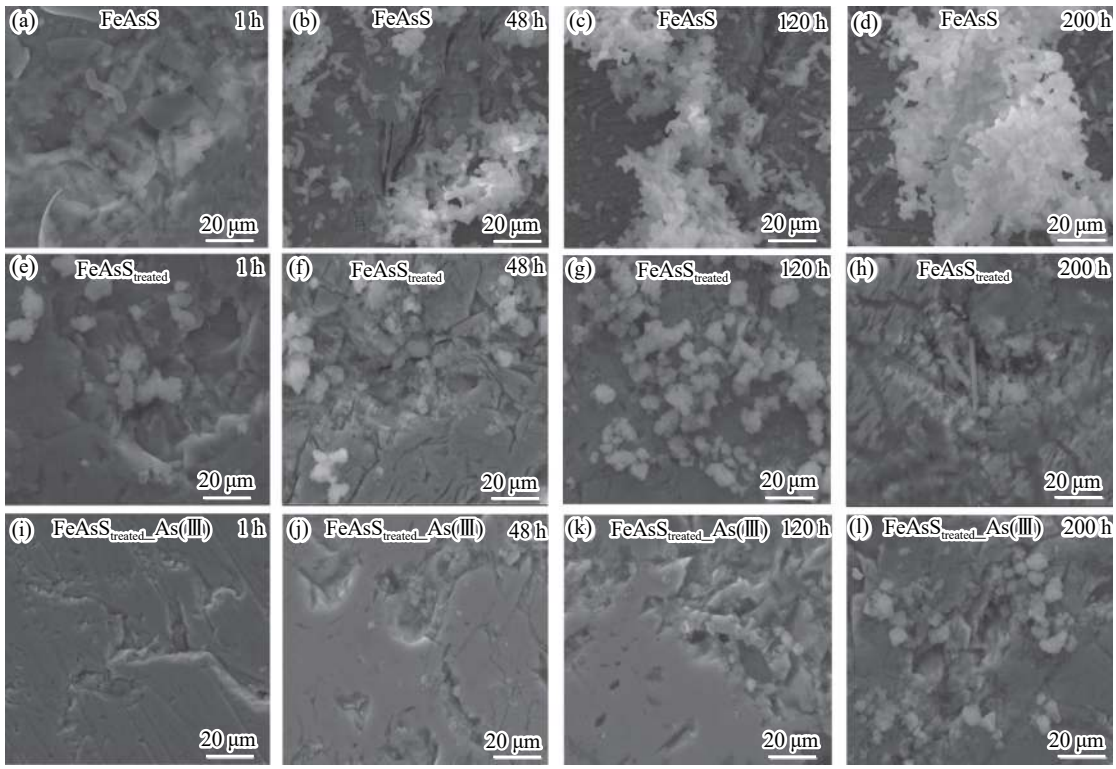

Fig. 4. SEM images of attachment results on the different arsenopyrite slice surfaces by *S. thermosulfidooxidans* FeAsS (a–d), FeAsS$_{treated}$ (e–h), and FeAsS$_{treated}$_As(III) (i–l).

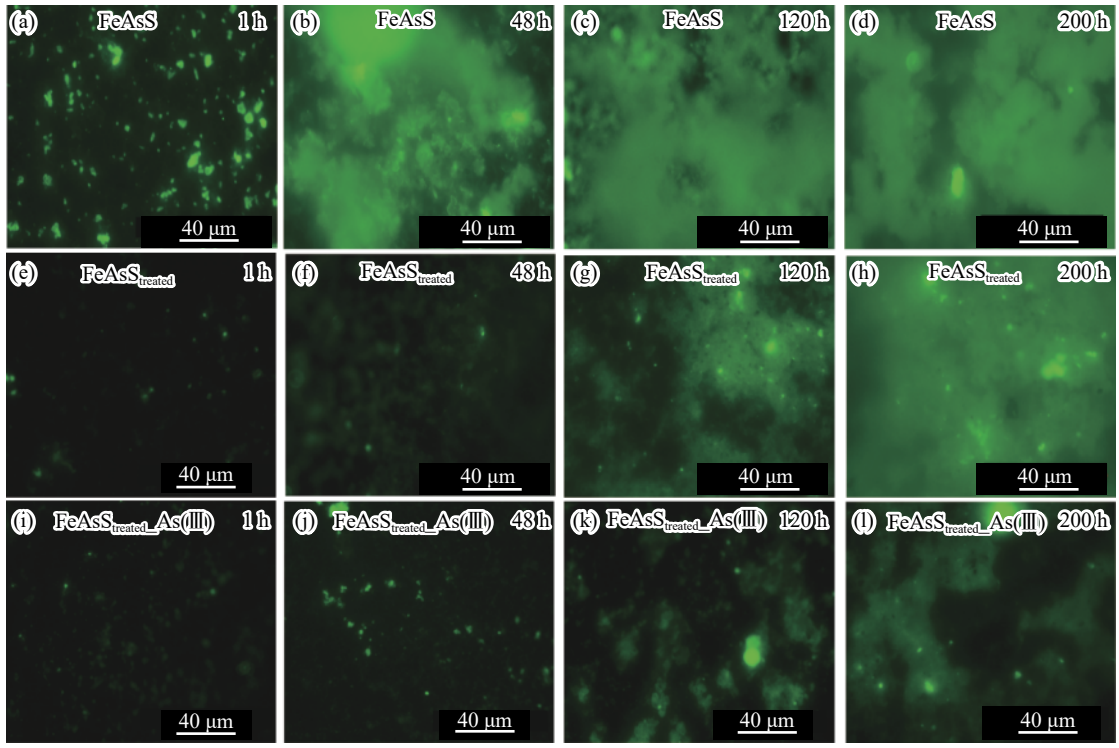

Fig. 5. EFM images of FITC-labeled *S. thermosulfidooxidans* cells adsorbed for different times on the arsenopyrite surfaces for FeAsS (a–d), FeAsS$_{treated}$ (e–h), FeAsS$_{treated}$_As(III) (i–l).

creased from 1 to 48 h. Biofilm formed at 48 h, followed by a slight decrease in fluorescence intensity. Compared with the biofilm formed on the original arsenopyrite surface, the biofilm in Figs. 5(e)–5(h) was different; at 1 and 48 h, there

were no obvious fluorescence, indicating that the surface deficient in S led to lower cell adsorption. The fluorescence intensity and area on the arsenopyrite surface in the As(III) system (Figs. 5(i)–5(l)) was less than the other two groups. At 120 h, the adsorption of bacteria on its surface also increased significantly (Fig. 5(k)), which is consistent with the sudden increase in C content at 120 h, as shown in Table 1.

The nucleic acid of bacterial cells was labeled with DAPI to represent the number of adsorbed bacteria cells, and the results are shown in Fig. 6. The overall change is similar to Fig. 5. The adsorption of bacterial cells on the arsenopyrite surfaces increased with time: from point shape, part of the sheet shape, to the biofilm. Notably, the formation of biofilm on corroded slice surfaces (Figs. 6(e)–6(h)) was more regular from 1 to 200 h. The area of biofilm in Figs. 6(i)–6(l) was less than Figs. 6(e)–6(h); however, the fluorescence intensity was stronger than Figs. 6(a)–6(d), which may be because As(III) was toxic to cells and inhibited biofilm formation and expansion, resulting in greatly improved resistance capacity of bacterial cells after the selection of As(III). Therefore, the nucleic acid fluorescence intensity was stronger.

3.5. Sulfur speciation on the arsenopyrite surface

The S K-edge XANES results of arsenopyrite slice samples are shown in Fig. 7. Fig. 7(a) shows that the S K-edge XANES spectra of referenced samples were significantly different in their peak positions and intensities. For the bioleaching groups of FeAsS (Fig. 7(b)), without $NaAsO_2$ (Fig. 7(c)) and with $NaAsO_2$ (Fig. 7(d)), the intensity of the characteristic peak (at 2.4724 keV) of arsenopyrite decreased with time and the peak intensity at 2.4826 keV corresponding to SO_4^{2-} increased. However, the decrease in the intensities of peaks of arsenopyrite were not obvious in the experiment with $NaAsO_2$, and the intensities of peaks of SO_4^{2-} increased significantly at 200 h.

Table 2 further shows that the sulfur species of the surface of arsenopyrite slices of FeAsS, FeAsS treated electrochemically without, and with As(III) at 48 h were mainly composed of 79.2% arsenopyrite, 10.8% S^0,10% SO_4^{2-}, 34.5% arsenopyrite, 45.9% S^0, 15.3% SO_4^{2-}, 4.3% SO_3^{2-},50.4% arsenopyrite, 46.9% S^0, 2.7% SO_4^{2-}, respectively. These results demonstrate that the addition of As(III) affects the metabolism of bacteria. The content of arsenopyrite decreased, while the sulfur species changed. At 120 h, the surface sulfur species were composed of 58.1% arsenopyrite, 32.5% S^0, 7.6% SO_4^{2-}, 1.8% $Na_2S_2O_3$ for the $FeAsS_{untreated}$ group; 49.2% S^0, 42.7% SO_4^{2-}, 2.4% $Na_2S_2O_3$, 5.7% SO_3^{2-} for the $FeAsS_{treated}$ group; 49.2% arsenopyrite, 43.3% S^0, 7.5% SO_4^{2-} for the $FeAsS_{treated}$_As(III) group, respectively. The results suggest that the electrochemical treatment promoted the dissolution of the minerals and produced more elemental sulfur and sulfate minerals (schwertmannite and jarosite). Arsenopyrite is barely detectable at 120 h on the surface of treated arsen-

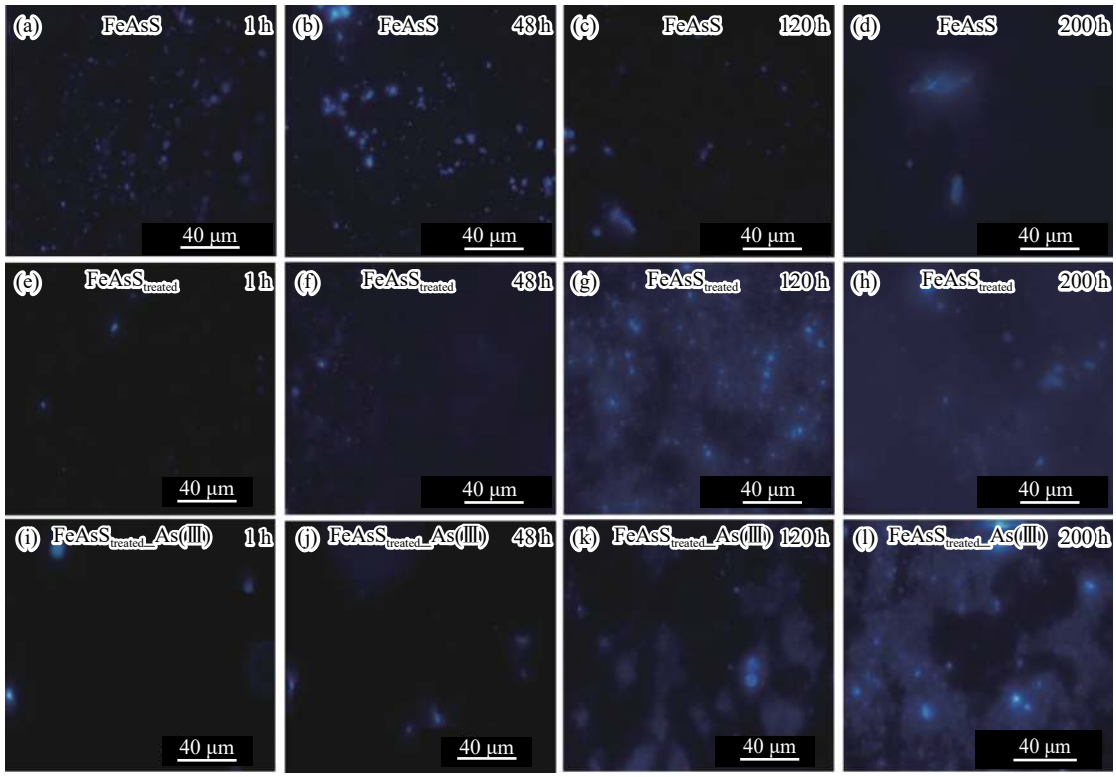

Fig. 6. The EFM images of DAPI-labeled *S. thermosulfidooxidans* cells adsorbed for different times on the FeAsS (a–d), $FeAsS_{treated}$ (e–h), and $FeAsS_{treated}$_As(III) arsenopyrite slices (i–l).

Table 2. The fitted S-K XANES results for Fig. 7.

Sample	Time / h	Percentage of contribution of reference spectra / mol%				
		FeAsS	S^0	SO_4^{2-}	$Na_2S_2O_3$	Na_2SO_3
FeAsS	1	89.4	3.4	7.2	—	—
	48	79.2	10.8	10	—	—
	120	58.1	32.5	7.6	1.8	—
	200	20.6	55	22.5	1.9	—
$FeAsS_{treated}$	1	57.9	32.5	7.8	1.8	—
	48	34.5	45.9	15.3	—	4.3
	120	—	49.2	42.7	2.4	5.7
	200	—	55.1	42.9	2.0	—
$FeAsS_{treated}$_As(III)	1	87.7	4.6	4.1	3.5	—
	48	50.4	46.9	2.7	—	—
	120	49.2	43.3	7.5	—	—
	200	55.5	32.3	11.6	5	—

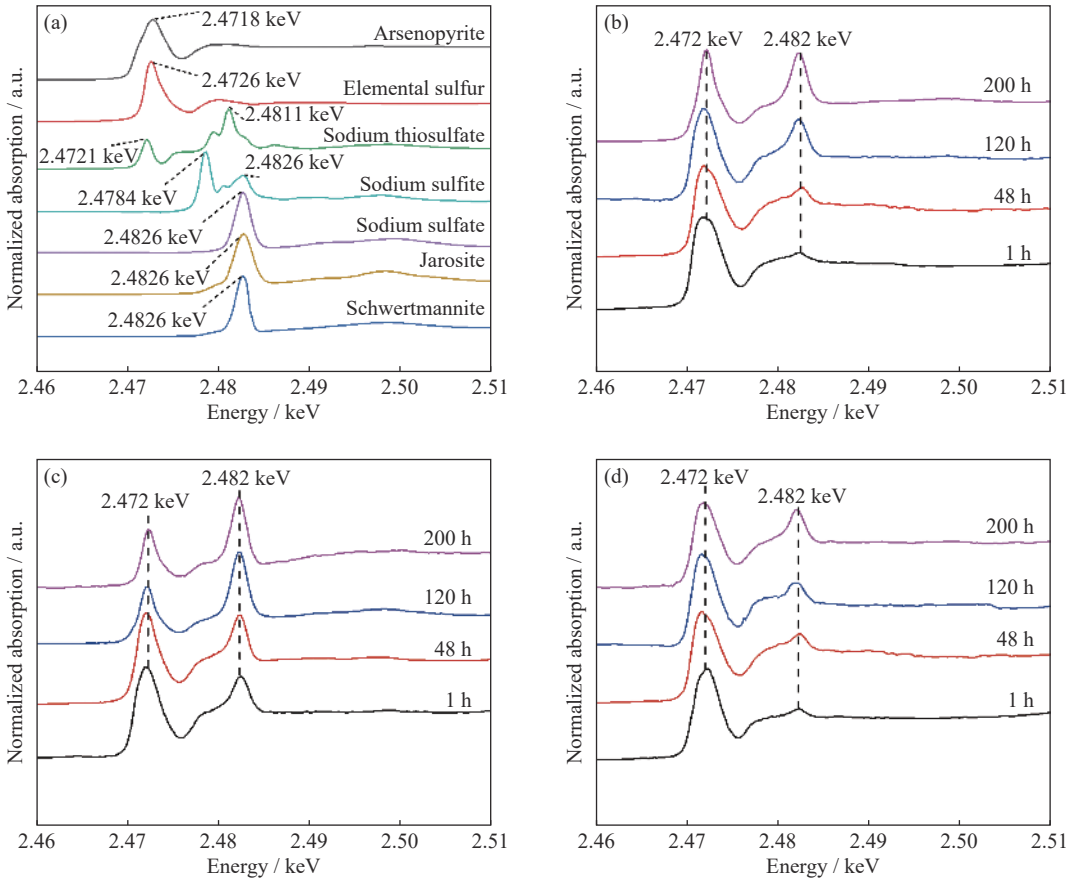

Fig. 7. The S K-edge XANES of arsenopyrite surfaces with bioleaching time with standards (a), FeAsS (b), treated FeAsS (c), and treated FeAsS with As(III) (d).

opyrite, which may indicate biofilm is too thick to cover the arsenopyrite surface.

4. Discussion

In this study, the surface with crystal defects caused by electrochemical corrosion attracted more cells attachment. After electrochemical treatment, there were obvious gullies on the surface of the arsenopyrite, and the chemical composition was changed, forming a Fe/S-deficient surface (Fig. 2). The crystal lattice defects of the mineral surface (caused by different causes) can affect the attachment behavior of cells because a surface with crystal defects is more readily attacked by H^+ [11,36–37], the iron on the arsenopyrite surface

can be released into solution as Fe^{2+}, which is then oxidized to Fe^{3+} by the planktonic cells in the solution, as shown in Eqs. (1)–(2). Through the above process, the surface of mineral corrosion is eroded by ferric iron ions, forming ferrous iron ions and S^0 as in Eq. (3) [38].

$$4FeAsS + 3O_2 + 2H_2O \rightarrow 4HAsO_2 + 4Fe^{2+} + 4S^0_{surface} \quad (1)$$

$$4Fe^{2+} + 4H^+ + O_2 \rightarrow 4Fe^{3+} + 2H_2O \quad (2)$$

$$FeAsS + 7Fe^{3+} + 4H_2O \rightarrow H_3AsO_4 + 8Fe^{2+} + S^0_{surface} + 5H^+ \quad (3)$$

The structure and evolution of biofilms depend on the properties of the substrate and its electrochemical properties [16,39–40]. After electrochemical corrosion at 1.21 V, arsenopyrite surfaces in the presence of surface sulfur compounds (i.e., S_n^{2-}/S^0) are beneficial to the development of biofilm [41], and the metabolic capacity of *A. thiooxidans* was then stimulated by the presence of S_n^{2-} and S^0 compounds on the extracellular surfaces, allowing colonization of the substrate [16]. However, in this study, after electrochemical corrosion at 0.26 V, the surface that was deficient in S and Fe was not conductive to the initial adsorption of bacterial cells (Fig. 5(b), Fig. 6(b)).

By contrast, a solid phase of arsenic was essentially innocuous to biofilm evolution with soluble species, [42–43]. According to the EFM images of FITC analyses, the adsorption number of cells on the arsenopyrite surface increased, and the biofilm formed at 48 h, while with increasing time, the fluorescence intensity on the arsenopyrite surface decreased for the experiment without dissolved As(III) (Figs. 5(a)–5(d)), which may be because the biofilm formation entered the later stage, and cells gradually diffused and detached from the mineral surface [44]. However, for the experiment with As(III), the initial adsorption of the bacteria was significantly inhibited by As(Ⅲ), and the adsorption increased when the bacteria adapted to the environment containing As(Ⅲ).

The adverse effect (damage) of As during biofilm evolution was in agreement with previous analyses and reports [18,41–42,45]. Results in Figs. 4(i)–4(l) and Figs. 5(i)–5(l) show that added As(III) inhibited the biofilm formation on the arsenopyrite surface. Figs. 4(i)–4(l) show that the adsorption of bacteria was mainly in the uneven area and there was no obvious biofilm formation; however, some attached, spread cells were observed at 120 h. According to the EDS analyses, the content of C in the groups of $FeAsS_{treated}$ and $FeAsS_{treated}$_As(III) was the lowest (Table 1), indicating that As(III) was more toxic and excessive As(III) severely inhibited bacterial attachment. The presence of As(III) likely inhibits the iron sulfur oxidation activity of leaching microorganisms and the growth of bacterial cells [46–47], which also affects the interactions between the microbe and minerals.

By considering the crystal chemical characteristics of sulfide minerals, Jia *et al*. [48] analyzed the relationship between the surface characteristics of the cracked surface of four kinds of sulfide minerals and the selective adsorption of bacteria, demonstrating that the types of metal ions on the fracture surface of minerals were the primary elements that induce the selective adsorption of microorganisms. Additionally, the distribution and properties of metal ions and sulfur exposed on the surface of minerals directly affected the adsorption amount of cells on the surface of minerals, which were the primary factors that induced the selective adsorption of cells. The EDS results (Table 1) demonstrate that in the initial adsorption process, arsenopyrite cannot meet the demand of *S. thermosulfidooxidans* for energy substrates because of the lack of S and Fe, thus influencing the interaction of *S. thermosulfidooxidans* and arsenopyrite to reduce the adsorption quantities.

The formation of secondary minerals on the mineral surface also has an important influence on the adsorption of bacterial cells. For example, the reduced sulfur as an important energy substrate is of great significance to the growth of bacterial cells. The sulfur K-edge XANES analysis in this study showed that the electrochemical treatment promoted the formation of S^0 and sulfate minerals (schwertmannite and jarosite), which contributed to the rapid formation of biofilm on the arsenopyrite surface (Figs. 5(a)–5(d), 6(a)–6(d)). Additionally, potentiostatixc oxidation on the surface of arsenopyrite can rapidly produce surface sulfur compounds (i.e., S_n^{2-}/S^0), which promote the development of a biofilm in the later [41]. However, according to Ramírez-Aldaba *et al*. [16], the addition of As(Ⅴ) did not hinder biofilm formation, which is different with the addition of As(III) that leads to significant inhibition of biofilm formation. These results demonstrate that the attachment of cells and the growth of the biofilm on the moderate thermophile *S. thermosulfidooxidans* are affected by the surface structure chemical speciation of minerals and by arsenic species.

5. Conclusions

The surface structure of arsenopyrite has defects after electrochemical treatment, with a 0.26 V treatment resulting in a distinct S and Fe deficiencies. The absence of S and Fe was not conducive to the initial attachment of bacterial cells and the attachment mainly occurred at the defect. When As(Ⅲ) was added, the bacterial cells showed a short stasis period and metabolic activity was inhibited. The bacterial attachment mainly occurred in the gully region throughout the entire phase. This study indicates that the surface microstructure and the addition of As(Ⅲ) significantly affected the adsorption behavior and biofilm formation of bacteria on the surface of arsenopyrite, which is helpful to understanding the mechanism of microbe–mineral interfacial interactions in the presence of As(III) in an AMD environment.

Acknowledgements

This work was financially supported by National Natural Science Foundation of China (Nos. 51774342, 41802038, U1608254, 51861135305, and 41830318) and Beijing Synchrotron Radiation Facility Public User Program (2018-BEPC-PT-002240).

References

[1] C.L. Corkhill and D.J. Vaughan, Arsenopyrite oxidation—A review, *Appl. Geochem.*, 24(2009), No. 12, p. 2342.

[2] D.M. Miller and G.S. Hansford, Batch biooxidation of a gold-bearing pyrite-arsenopyrite concentrate, *Miner. Eng.*, 5(1992), No. 6, p. 613.

[3] F. Espiell, A. Roca, M. Cruells, and C. Núñez, Gold and silver recovery by cyanidation of arsenopyrite ore, *Hydrometallurgy*, 16(1986), No. 2, p. 141.

[4] H.R. Watling, The bioleaching of sulphide minerals with emphasis on copper sulphides—A review, *Hydrometallurgy*, 84(2006), No. 1-2, p. 81.

[5] S.F. Wang, B.B. Jiao, M.M. Zhang, G.Q. Zhang, X. Wang, and Y.F. Jia, Arsenic release and speciation during the oxidative dissolution of arsenopyrite by O_2 in the absence and presence of EDTA, *J. Hazard. Mater.*, 346(2018), p. 184.

[6] J.S. Liu, Z.H. Wang, M.M. Gen, and G.Z. Qiu, Progress in the study of polyphase interfacial interactions between microorganism and mineral in bio-hydrometallurgy, *Min. Metall. Eng.*, 26(2006), No. 1, p. 40.

[7] W.B. Ling, L. Wang, H.C. Liu, Z.Y. Nie, Y. Yang, Y. Yang, C.Y. Ma, L. Zheng, Y.D. Zhao, and J.L. Xia, The evidence of decisive effect of both surface microstructure and speciation of chalcopyrite on attachment behaviors of extreme thermoacidophile sulfolobus metallicus, *Minerals*, 8(2018), No. 4, art. No. 159.

[8] G. Vander Voort, Color metallography, *Microsc. Microanal.*, 10(2004), No. S02, p. 70.

[9] R.Y. Zhang, T.R. Neu, S. Bellenberg, U. Kuhlicke, W. Sand, and M. Vera, Use of lectins to *in situ* visualize glycoconjugates of extracellular polymeric substances in acidophilic archaeal biofilms, *Microb. Biotechnol.*, 8(2015), No. 3, p. 448.

[10] M. Vera, A. Schippers, and W. Sand, Progress in bioleaching: Fundamentals and mechanisms of bacterial metal sulfide oxidation—part A, *Appl. Microbiol. Biotechnol.*, 97(2013), No. 17, p. 7529.

[11] J.L. Xia, H.R. Zhu, L. Wang, H.C. Liu, Z.Y. Nie, Y.D. Zhao, C.Y. Ma, C.H. Hong, and X.J. Zhen, *In situ* characterization of relevance of surface microstructure and electrochemical properties of chalcopyrite to adsorption of Acidianus manzaensis, *Adv. Mater. Res.*, 1130(2015), p. 183.

[12] D.W. Price and G.W. Warren, The influence of silver ion on the electrochemical response of chalcopyrite and other mineral sulfide electrodes in sulfuric acid, *Hydrometallurgy*, 15(1986), No. 3, p. 303.

[13] W. Sand, T. Gehrke, P.G. Jozsa, and A. Schippers, (Bio)chemistry of bacterial leaching—direct vs. indirect bioleaching, *Hydrometallurgy*, 59(2001), No. 2-3, p. 159.

[14] R.H. Lara, J.V. García-Meza, I. González, and R. Cruz, Influence of the surface speciation on biofilm attachment to chalcopyrite by Acidithiobacillus thiooxidans, *Appl. Microbiol. Biotechnol.*, 97(2013), No. 6, p. 2711.

[15] R.H. Lara, D. Valdez-Pérez, A.G. Rodríguez, H.R. Navarro-Contreras, R. Cruz, and J.V. García-Meza, Interfacial insights of pyrite colonized by Acidithiobacillus thiooxidans cells under acidic conditions, *Hydrometallurgy*, 103(2010), No. 1-4, p. 35.

[16] H. Ramírez-Aldaba, J. Vázquez-Arenas, F.S. Sosa-Rodríguez, D. Valdez-Pérez, E. Ruiz-Baca, G. Trejo-Córdoba, M.A. Escobedo-Bretado, L. Lartundo-Rojas, P. Ponce-Peña, and R.H. Lara, Changes in biooxidation mechanism and transient biofilm characteristics by As(V) during arsenopyrite colonization with Acidithiobacillus thiooxidans, *J. Ind. Microbiol. Biotechnol.*, 45(2018), No. 8, p. 669.

[17] N. Yee, J.B. Fein, and C.J. Daughney, Experimental study of the pH. ionic strength.and reversibility behavior of bacteria-mineral adsorption, *Geochim. Cosmochim. Acta*, 64(2000), No. 4, p. 609.

[18] S. Koechler, J. Farasin, J. Cleiss-Arnold, and F. Arsène-Ploetze, Toxic metal resistance in biofilms: Diversity of microbial responses and their evolution, *Res. Microbiol.*, 166(2015), No. 10, p. 764.

[19] J.J. Harrison, H. Ceri, C.A. Stremick, and R.J. Turner, Biofilm susceptibility to metal toxicity, *Environ. Microbiol.*, 6(2004), No. 12, p. 1220.

[20] R.J. Ram, N.C. Verberkmoes, M.P. Thelen, G.W. Tyson, B.J. Baker, R.C. Blake, M. Shah, R.L. Hettich, and J.F. Banfield, Community proteomics of a natural microbial biofilm, *Science*, 308(2005), No. 5730, p. 1915.

[21] Geochim. Cosmochim. Acta, Is arsenic biotransformation a detoxification mechanism for microorganisms?, *Aquat. Toxicol.*, 146(2014), p. 212.

[22] H.C. Liu, *Study on the Interfacial Interactions Between Bioleaching Microorganisms and Sulfur-Containing Substrates and Their Molecular Mechanism* [Dissertation], Central South University, Changsha, 2016, p. 82.

[23] D.R. Zhang, J.L. Xia, Z.Y. Nie, H.R. Chen, H.C. Liu, Y. Deng, Y.D. Zhao, L.L. Zhang, W. Wen, and H.Y. Yang, Mechanism by which ferric iron promotes the bioleaching of arsenopyrite by the moderate thermophile Sulfobacillus thermosulfidooxidans, *Process. Biochem.*, 81(2019), p. 11.

[24] D.R. Zhang, H.R. Chen, J.L. Xia, Z.Y. Nie, X.L. Fan, H.C. Liu, L. Zheng, L.J. Zhang, and H.Y. Yang, Humic acid promotes arsenopyrite bio-oxidation and arsenic immobilization, *J. Hazard. Mater.*, 384(2020), art. No. 121359.

[25] Q. Li, R.Y. Zhang, B.A. Krok, M. Vera, and W. Sand, Biofilm formation of Sulfobacillus thermosulfidooxidans on pyrite in the presence of Leptospirillum ferriphilum, *Adv. Mater. Res.*, 1130(2015), p. 141.

[26] T.Y. Gu, S.O. Rastegar, S.M. Mousavi, M. Li, and M.H. Zhou, Advances in bioleaching for recovery of metals and bioremediation of fuel ash and sewage sludge, *Bioresour. Technol.*, 261(2018), p. 428.

[27] K.O. Stetter, A. Segerer, W. Zillig, G. Huber, G. Fiala, R. Huber, and H. König, Extremely thermophilic sulfur-metabolizing archaebacteria, *Syst. Appl. Microbiol.*, 7(1986), No. 2-3, p. 393.

[28] K. Bosecker, Bioleaching: metal solubilization by microorganisms, *FEMS Microbiol. Rev.*, 20(1997), No. 3-4, p. 591.

[29] C.L. Liang, J.L. Xia, Y. Yang, Z.Y. Nie, X.J. Zhao, L. Zheng, C.Y. Ma, and Y.D. Zhao, Characterization of the thermo-reduction process of chalcopyrite at 65°C by cyclic voltammetry and XANES spectroscopy, *Hydrometallurgy*, 107(2011), No. 1-2, p. 13.

[30] C. Castro, R.Y. Zhang, J. Liu, S. Bellenberg, T.R. Neu, E.

Donati, W. Sand, and M. Vera, Biofilm formation and interspecies interactions in mixed cultures of thermo-acidophilic archaea Acidianus spand Sulfolobus metallicus, *Res. Microbiol.*, 167(2016), No. 7, p. 604.

[31] A. Koerdt, J. Gödeke, J. Berger, K.M. Thormann, and S.V. Albers, Crenarchaeal biofilm formation under extreme conditions, *PLoS One*, 5(2010), No. 11, art. No. e14104.

[32] C.J. de Africa, R.P. van Hille, W. Sand, and S.T.L. Harrison, Investigation and *in situ* visualisation of interfacial interactions of thermophilic microorganisms with metal-sulphides in a simulated heap environment, *Miner. Eng.*, 48(2013), p. 100.

[33] J.L. Xia, Y. Yang, H. He, C.L. Liang, X.J. Zhao, L. Zheng, C.Y. Ma, Y.D. Zhao, Z.Y. Nie, and G.Z. Qiu, Investigation of the sulfur speciation during chalcopyrite leaching by moderate thermophile Sulfobacillus thermosulfidooxidans, *Int. J. Miner. Process.*, 94(2010), No. 1-2, p. 52.

[34] A. Ide-Ektessabi, T. Kawakami, and F. Watt, Distribution and chemical state analysis of iron in the Parkinsonian substantia nigra using synchrotron radiation micro beams, *Nucl. Instrum. Methods Phys. Res., Sect. B*, 213(2004), p. 590.

[35] B. Ravel and M. Newville, Athena, Artemis, Hephaestus: Data analysis for X-ray absorption spectroscopy using IFEFFIT, *J. Synchrotron Radiat.*, 12(2005), No. 4, p. 537.

[36] N. Noël, B. Florian, and W. Sand, AFM & EFM study on attachment of acidophilic leaching organisms, *Hydrometallurgy*, 104(2010), No. 3-4, p. 370.

[37] R.Y. Zhang, M. Vera, S. Bellenberg, and W. Sand, Attachment to minerals and biofilm development of extremely acidophilic archaea, *Adv. Mater. Res.*, 825(2013), p. 103.

[38] M.G.M. Fernandez, C. Mustin, P. de Donato, O. Barres, P. Marion, and J. Berthelin, Occurrences at mineral-bacteria interface during oxidation of arsenopyrite by Thiobacillus ferrooxidans, *Biotechnol. Bioeng.*, 46(1995), No. 1, p. 13.

[39] R.M. Donlan, Biofilms: microbial life on surfaces, *Emerg. Infect. Dis.*, 8(2002), No. 9, p. 881.

[40] A. Echeverría-Vega and C. Demergasso, Copper resistance, motility and the mineral dissolution behavior were assessed as novel factors involved in bacterial adhesion in bioleaching, *Hydrometallurgy*, 157(2015), p. 107.

[41] H. Ramírez-Aldaba, O.P. Valles, J. Vazquez-Arenas, J.A. Rojas-Contreras, D. Valdez-Pérez, E. Ruiz-Baca, M. Meraz-Rodríguez, F.S. Sosa-Rodríguez, Á.G. Rodríguez, and R.H. Lara, Chemical and surface analysis during evolution of arsenopyrite oxidation by Acidithiobacillus thiooxidans in the presence and absence of supplementary arsenic, *Sci. Total Environ.*, 566-567(2016), p. 1106.

[42] F.F. Leng, K.Y. Li, X.X. Zhang, Y.Q. Li, Y. Zhu, J.F. Lu, and H.Y. Li, Comparative study of inorganic arsenic resistance of several strains of Acidithiobacillus thiooxidans and Acidithiobacillus ferrooxidans, *Hydrometallurgy*, 98(2009), No. 3-4, p. 235.

[43] J. Jin, S.Y. Shi, G.L. Liu, Q.H. Zhang, and W. Cong, Arsenopyrite bioleaching by Acidithiobacillus ferrooxidans in a rotating-drum reactor, *Miner. Eng.*, 39(2012), p. 19.

[44] R.Y. Zhang, S. Bellenberg, L. Castro, T.R. Neu, W. Sand, and M. Vera, Colonization and biofilm formation of the extremely acidophilic archaeon Ferroplasma acidiphilum, *Hydrometallurgy*, 150(2014), p. 245.

[45] S.R. Dave, K.H. Gupta, and D.R. Tipre, Characterization of arsenic resistant and arsenopyrite oxidizing Acidithiobacillus ferrooxidans from Hutti gold leachate and effluents, *Bioresour. Technol.*, 99(2008), No. 16, p. 7514.

[46] K.B. Hallberg, H.M. Sehlin, and E.B. Lindström, Toxicity of arsenic during high temperature bioleaching of gold-bearing arsenical pyrite, *Appl. Microbiol. Biotechnol.*, 45(1996), No. 1-2, p. 212.

[47] B. Escobar, E. Huenupi, I. Godoy, and J.V. Wiertz, Arsenic precipitation in the bioleaching of enargite by Sulfolobus BC at 70°C, *Biotechnol. Lett.*, 22(2000), No. 3, p. 205.

[48] C.Y. Jia, D.Z. Wei, W.G. Liu, C. Han, S.L. Gao, and Y.J. Wang, Selective adsorption of bacteria on sulfide minerals surface, *Trans. Nonferrous Met. Soc. China*, 18(2008), No. 5, p. 1247.